Neuro-Oncology 13(2):251–260, 2011.
doi:10.1093/neuonc/noq172
Advance Access publication December 16, 2010

Magnetic resonance imaging of intracranial tumors: intra-patient comparison of gadoteridol and ferumoxytol

Edit Dósa, Daniel J. Guillaume, Marianne Haluska, Cynthia A. Lacy, Bronwyn E. Hamilton, Jeffrey M. Njus, William D. Rooney, Dale F. Kraemer, Leslie L. Muldoon, and Edward A. Neuwelt

Department of Neurology (E.D., M.H., C.A.L., L.L.M., E.A.N.), Department of Neurosurgery (D.J.G., E.A.N.), Department of Radiology (B.E.H.), Department of Public Health and Preventive Medicine (D.F.K.), Department of Medical Informatics and Clinical Epidemiology (D.F.K.), Advanced Imaging Research Center (J.M.N., W.D.R.), Oregon Health and Science University, Portland, Oregon Department of Pharmacy Practice, Oregon State University, Portland, Oregon (D.F.K.); Portland Veterans Affairs Medical Center, Portland, Oregon (E.A.N)

This study aims to compare gadoteridol with ferumoxytol for contrast-enhanced and perfusion-weighted (PW) MRI of intracranial tumors. The final analysis included 26 patients, who underwent 3 consecutive days of 3T MRI. Day 1 consisted of anatomical pre- and postcontrast images, and PW MRI was acquired using gadoteridol (0.1 mmol/kg). On Day 2, the same MRI sequences were obtained with ferumoxytol (510 mg) and on Day 3, the anatomical images were repeated to detect delayed ferumoxytol-induced signal changes. The T_1-weighted images were evaluated qualitatively and quantitatively for enhancement volume and signal intensity (SI) changes; PW data were used to estimate the relative cerebral blood volume (rCBV). All 26 lesions showed 24-hour T_1-weighted ferumoxytol enhancement; 16 also had T_2-weighted hypointensities. In 6 patients, ferumoxytol-induced signal changes were noted in areas with no gadoteridol enhancement. Significantly greater ($P < .0001$) SI changes were seen with gadoteridol, and qualitative analyses (lesion border delineation, internal morphology, contrast enhancement) also showed significant preferences ($P = .0121$; $P = .0015$; $P < .0001$, respectively) for this agent. There was no significant difference in lesion enhancement volumes between contrast materials. The ferumoxytol-rCBV values were significantly higher ($P = .0016$) compared with the gadoteridol-rCBV values. In conclusion, ferumoxytol provides important information about tumor biology that complements gadoteridol imaging. The rCBV measurements indicate areas of tumor undergoing rapid growth, whereas the 24-hour scans mark the presence of inflammatory cells. Both of these functions provide useful information about tumor response to treatment. We suggest that dynamic and anatomical imaging with ferumoxytol warrant further assessment in brain tumor therapy.

Keywords: brain tumors, ferumoxytol, magnetic resonance imaging, ultrasmall superparamagnetic iron oxide nanoparticles.

The most commonly used gadolinium-based contrast agents (GBCAs) are low-molecular-weight extracellular substances with a short plasma half-life. GBCAs are relatively safe when administered in clinically recommended doses (0.1–0.3 mmol/kg). However, emerging evidence linking GBCAs to nephrogenic systemic fibrosis has changed medical practice patterns toward avoiding gadolinium-enhanced MRI in patients with glomerular filtration rates (GFR) < 30 mL/min/1.73m^2.[1]

Ultrasmall superparamagnetic iron oxide nanoparticles (USPIOs), such as ferumoxytol (Feraheme, AMAG Pharmaceuticals Inc.), developed for iron-replacement therapy primarily in patients with kidney disease, are promising contrast materials for brain tumor MRI due to their T_1 and T_2 relaxation time—shortening effects.[2,3] The semisynthetic carbohydrate-coated

Received June 8, 2010; accepted September 30, 2010.

Corresponding Author: Edward A. Neuwelt, MD, Oregon Health and Science University, 3181 S.W. Sam Jackson Park Road, L603, Portland, OR 97239-3098 (neuwelte@ohsu.edu).

ferumoxytol, which has a hydrodynamic diameter of 30 nm, shows little uptake by circulating monocytes, resulting in a long blood half-life (14 hours).[4] Ferumoxytol can be safely given as a short intravenous bolus for dynamic MRI where it serves as a true blood pool agent at early time points (minutes) and is useful for measurement of the relative cerebral blood volume (rCBV).[5,6] Over a period of hours, ferumoxytol undergoes uptake in reactive astrocytes and tissue macrophages.[7] Consequently, ferumoxytol has the potential for imaging of both tumor vasculature and inflammation in central nervous system (CNS) malignancies.[7,8]

A 1.02-g treatment course of ferumoxytol (2 × 510 mg) was used for iron-replacement therapy in a large number of patients without significant adverse effects.[9] So far, the highest given dose of ferumoxytol as an MRI contrast agent was 4 mg/kg (280 mg for a 70-kg patient).[3] A total dose of 510 mg (the maximum FDA-approved dose) of ferumoxytol administered in this study has not been investigated for MR imaging before. This study aims to qualitatively and quantitatively compare gadoteridol (ProHance, Bracco Diagnostic Inc.) with high-dose ferumoxytol for contrast-enhanced and perfusion-weighted (PW) MRI in patients with intracranial tumors.

Subjects and Methods

Study Population

Between March 2008 and February 2010, 36 patients with intracranial tumors were enrolled in this prospective study. Patients who were younger than 18 years; were pregnant or lactating; showed clinical symptoms and signs of herniation (e.g. acute pupillary enlargement, rapidly developing motor changes, rapidly decreasing level of consciousness) or hemodynamic instability; had contraindications to MRI procedures (e.g. pacemaker); or had known allergic or hypersensitivity reactions to parenteral iron, dextran, iron-dextran or iron-polysaccharide preparations; had known or suspected iron overload (e.g. hemochromatosis, history of multiple transfusions); or had hepatic insufficiency or liver cirrhosis were excluded. HIV-positive patients on combination antiretroviral therapy were also ineligible because of the potential for pharmacokinetic interactions with ferumoxytol.

The study was sponsored by the National Institutes of Health and was approved by the Oregon Health and Science University Institutional Review Board (eIRB #1562). All participants provided written informed consent.

MRI Examination

All MRI scans were performed on a 3T whole-body MRI system (TIM Trio, Siemens) with a body radio frequency (RF) coil transmit and a 12-channel phased-array head RF receiver coil. The imaging protocol consisted of 3 consecutive days. On the first day, localizer scout images, axial T_1- and T_2-weighted pre- and 18.5-minute (range, 16–21 minutes) postcontrast images, and first-pass dynamic susceptibility-weighted contrast-enhanced (DSC) perfusion MRI were acquired using gadoteridol gadolinium (III) chelate. On the following day, the same MRI sequences were obtained with ferumoxytol. On the third day, at least 22 hours (mean, 24.3 hours; range, 22–28 hours) after the USPIO agent administration, the anatomical images were repeated in identical spatial orientations to detect delayed ferumoxytol-induced signal changes. Subjects with renal insufficiency (GFR < 30 mL/min/1.73m^2) underwent only a 2-day MRI with USPIO, without gadoteridol.

Gadoteridol was injected at a dose of 0.1 mmol/kg of body weight. Ferumoxytol was given over 20 minutes in a constant volume of 17 mL (510 mg) diluted with 17 mL of saline regardless of body weight, from which a separate 5-mL bolus was used for DSC MRI. After contrast agent administration, the patients were monitored closely for 2 hours and were followed up for 1 month.

MRI Acquisition Parameters

To minimize possible differences, the inter-day MRI acquisitions were carefully repositioned using consistent and clearly visualized anatomical landmarks from high-quality scout MRI scans.

For T_1-weighted spin echo (SE) images, a repetition time (TR)/echo time (TE) of 900/10 was used, and up to 44 slices with a 2-mm^2 slice thickness without gap were obtained. A field of view (FOV) of 240 × 240 mm^2 and an acquisition matrix of 256 × 256 were chosen. For T_2-weighted turbo SE images, we used 9000/93 at a slice thickness of 2 mm^2 without gap. The TSE factor was 9, while the FOV was 240 × 240 mm^2 with an acquisition matrix of 256 × 256. For DSC MRI, dynamic T_2^*-weighted images were acquired using a gradient-echo echo-planar imaging pulse sequence (TR, 1500 ms; TE, 20 ms; FA, 45°; FOV, 192 × 192 mm^2; matrix, 64 × 64; and 27 interleaved slices with 3-mm^2 thickness and 0.9-mm^2 gap). After an initial baseline period of 7 series of 27 image slices (11 seconds), a rapid bolus of contrast agent was administered intravenously using a power injector (Spectris Solaris, Medrad Inc.) through an 18-gauge intravenous line at a rate of 3 mL/s, followed immediately by 20 mL of saline flush at the same rate. DSC data collection was continued for 90 series (2 minutes 21 seconds).

Image Analysis

All images from each patient were evaluated in a matched-pair fashion and were analyzed by two neuroradiologists in consensus. The image assessment consisted of the following steps:

(i) The total number of enhancing brain lesions as visualized on T_1-weighted gadoteridol-enhanced, T_1- and T_2-weighted ferumoxytol-enhanced images was recorded for each patient. In the case

of multiple lesions, only the largest, most conspicuous lesion was selected for further evaluation.

(ii) T_1-weighted gadoteridol and T_1-weighted 24-hour ferumoxytol enhancement patterns were compared in a descriptive manner. In addition, the images were scored in terms of the following: (1) lesion border delineation, (2) visualization of lesion internal morphology, and (3) lesion contrast enhancement compared with surrounding normal tissue. These assessments were performed by using 3-point scales from −1 (gadoteridol superior) through 0 (both contrast agents equal) to +1 (ferumoxytol superior).

(iii) T_1-weighted postcontrast (gadoteridol, 24-hour ferumoxytol) MR images were uploaded in MIPAV (Medical Image Processing, Analysis, and Visualization, BIRSS; NIH). The enhancing lesion was outlined on each MR image and the software calculated the enhancement volume. Volumetric analysis was expressed in units of cubic centimeter.

(iv) By using user-defined regions of interests (ROIs) in the lesion, contralateral normal brain parenchyma, and background noise, lesion-to-brain contrast-to-noise measurements for T_1-weighted pre- and postcontrast images were calculated as follows: $(SI_{lesion} - SI_{brain})/SI_{noise}$. On the basis of values recorded on T_1-weighted pre- and postcontrast (gadoteridol, 24-hour ferumoxytol) images, the percentage of signal intensity (SI) change in the lesion was calculated as follows: $[(SI_{postcontrast} - SI_{precontrast}) \times 100]/SI_{precontrast}$. ROIs of equal size were positioned at identical coordinates on all corresponding image sets. The ROIs were placed to encompass as much of the enhancing lesion as possible while avoiding necrosis or scarring within the lesion. The ROIs larger than 20 mm^2 were used to measure the SI of contralateral normal brain parenchyma and background noise. All SI measurements were made using ImageJ software (NIH).

(v) All first-pass DSC MRI data were processed using Lupe (Lund) perfusion image analysis software. The arterial input function was determined from the middle cerebral artery contralateral to the enhancing lesion. Color-coded rCBV maps were created on a voxel-wise basis uncorrected for contrast leakage and were overlaid onto T_1-weighted gadoteridol-enhanced images. Within the enhancing lesion, a single voxel ($3 \times 3 \times 3$ mm) ROI with the highest rCBV value was chosen on the ferumoxytol-rCBV parametric map. An ROI of equal size was positioned at identical coordinates on the gadoteridol-rCBV parametric map. ROI analyses were performed in native image space—an approach that is more labor-intensive but avoids interpolation errors frequently associated with rigid-body coregistration methods—using ImageJ software (NIH). Areas depicting major vessels were excluded from ROIs. Normal white matter within the contralateral hemisphere was used as the internal reference standard; rCBV values were calculated by dividing the maximal rCBV of the lesion by that of contralateral normal-appearing white matter.

Statistical Analysis

Categoric variables were presented as numbers. Continuous variables were expressed as means (standard errors), unless otherwise stated. The normality of distribution for all continuous variables was determined by the Kolmogorov–Smirnov test. The distribution of preferences for gadoteridol or ferumoxytol in various diagnostic information end-points (border delineation, visualization of lesion internal morphology, contrast enhancement) was tested using the Wilcoxon signed rank test. For enhancement volumes, SI changes, and rCBV ratios, the differences between the value using gadoteridol and the value using ferumoxytol were compared using paired *t*-tests. For contrast-to-noise ratios (CNRs), there were 3 groups of values (precontrast, gadoteridol, ferumoxytol) to compare; therefore, a mixed model, repeated measures analysis of variance (ANOVA) was performed, and multiple comparisons were made using the Tukey–Kramer adjustment if there was a significant difference among these values. All statistical computations were performed using SAS Version 9.2 for Windows (SAS Institute Inc.), and the results were declared significant at the two-sided 5% comparison-wise significance level ($P < .05$).

Results

Among 36 patients considered for inclusion in the study, no enhancing lesion was seen in 3 subjects with either gadoteridol or ferumoxytol. In 7 participants with end-stage renal disease or history of kidney transplantation, only ferumoxytol was used as a contrast agent. Therefore, 26 patients (18 men, 8 women; mean age, 47 years; age range, 19–72 years) were included for final comparative analysis. Twenty-three patients had histologically verified malignant brain tumors, including primary glial tumor ($n = 19$), angiocentric T-cell lymphoma ($n = 1$), and secondary metastasis ($n = 3$). Three patients had benign brain tumors [meningioma ($n = 2$), pituitary adenoma ($n = 1$)] (Table 1). All patients underwent surgery or biopsy 39.6 (3–255) [mean (range)] months before the study and 24 of them received 53.8 (0.5–61.5) [mean (range)] Gy fractionated external beam radiation therapy 31.7 (1–309) [mean (range)] months prior to study enrollment (Table 1). Ten out of 26 patients were treated with chemotherapy, 5 with bevacizumab (Avastin, Genentech; 5 or 10 mg/kg) alone or in combination with chemotherapeutic agents, and 11 were taking steroids (4–20 mg/day dexamethasone) at the time of the study (Table 1).

There were no adverse events attributed to either contrast material.

Table 1. Demographics and treatments

Patient No./ Gender/Age (years)	Histological Diagnosis	Treatment						
		Surgery		Radiation		Chemotherapeutic Agents	Steroids (mg/day)	Bevacizumab (mg/kg)
		Type	Time Interval (months)	Dose (Gy)	Time Interval (months)			
1/M/50	Glioblastoma multiforme	GTR	6	59.4	4	—	—	—
2/M/50	Glioblastoma multiforme	BX	9	59.4	7	C, T	4	10
3/F/46	Glioblastoma multiforme	STR	14	59.4	13	L	12	—
4/M/19	Glioblastoma multiforme	GTR	5	59.4	2	—	12	—
5/M/19	Glioblastoma multiforme	GTR	8	59.4	5	T	12	5
6/M/56	Glioblastoma multiforme	PR	32	59.4	29	T	—	—
7/F/57	Glioblastoma multiforme	GTR	9	59.4	6	T	—	—
8/F/57	Glioblastoma multiforme	GTR	12	59.4	9	T	—	—
9/M/54	Glioblastoma multiforme	PR	3	59.4	1	—	12	—
10/M/62	Glioblastoma multiforme	GTR	5	60	2	—	4	—
11/M/62	Glioblastoma multiforme	GTR	6	60	4	T	—	5
12/F/62	Glioblastoma multiforme	PR	7	60	3	T	8	—
13/M/32	Anaplastic oligodendroglioma	GTR	54	—	—	—	—	—
14/F/58	Anaplastic ependymoma	GTR	8	57.5	7	C	20	5
15/M/51	Anaplastic astrocytoma	BX	5	59.4	3	—	16	—
16/F/33	Anaplastic astrocytoma	BX	71	59.4	70	I	16	5
17/M/26	Pilocytic astrocytoma	PR	153	50.4	11	—	—	—
18/M/31	Astroblastoma	GTR	21	54	20	—	—	—
19/M/44	Pineoblastoma	GTR	87	50.4	72	—	—	—
20/M/46	Angiocentric T-cell lymphoma	BX	3	—	—	—	—	—
21/M/40	Nasopharyngeal carcinoma metastasis	BX	44	61.5	24	—	—	—
22/M/35	Melanoma metastasis	STR	28	48	28	—	—	—
23/F/72	Non small cell lung carcinoma metastasis	GTR	25	35	12	—	16	—
24/F/49	Meningioma	PR	255	50.4	309	—	—	—
25/M/53	Meningioma	STR	44	50.4	10	—	—	—
26/M/59	Non secreting pituitary adenoma	GTR	115	0.5	110	—	—	—

BX, biopsy; PR, partial resection; STR, subtotal resection; GTR, gross total resection C, carboplatin; I, irinotecan; L, lomustine; T, temozolomide.

Lesion Detection

All of the image sets from each of the 26 evaluated patients were technically adequate for assessment. Except for 2 patients, all participants had unifocal disease; in the 2 subjects with multifocal disease, only the largest most prominent lesion was assessed. T_1-weighted enhancement and/or T_2 signal dropout consistent with iron accumulation was detected in only 4 lesions within 29 minutes (mean, 25.2 minutes; range, 23–29 minutes) after ferumoxytol administration. All lesions showed 24-hour T_1 SI changes, but only 16 of them had T_2 hypointensities in the approximate region where gadoteridol enhancement was seen (Fig. 1A–H). The SI changes were more prominent and extended into a larger area on the 24-hour ferumoxytol-enhanced images compared with the 25-minute studies (Fig. 1C, D, G, and H). Six patients had ferumoxytol enhancement in areas that did not correspond to gadoteridol enhancement (Fig. 2).

Qualitative Image Assessment

Side-by-side analysis of T_1-weighted postcontrast images revealed that in 20 cases the lesions appeared more clearly after gadoteridol administration and the morphology of gadoteridol enhancement was more homogeneous compared with the hazy, punctate pattern of ferumoxytol enhancement (Fig. 3). In general, the ferumoxytol-induced hyperintense T_1 SI changes were readily detectable, while the hypointense T_2 SI changes were modest and more variable, but their volumes were relatively equivalent.

Comparison of T_1-weighted postcontrast images showed highly significant preferences ($P = .0121$;

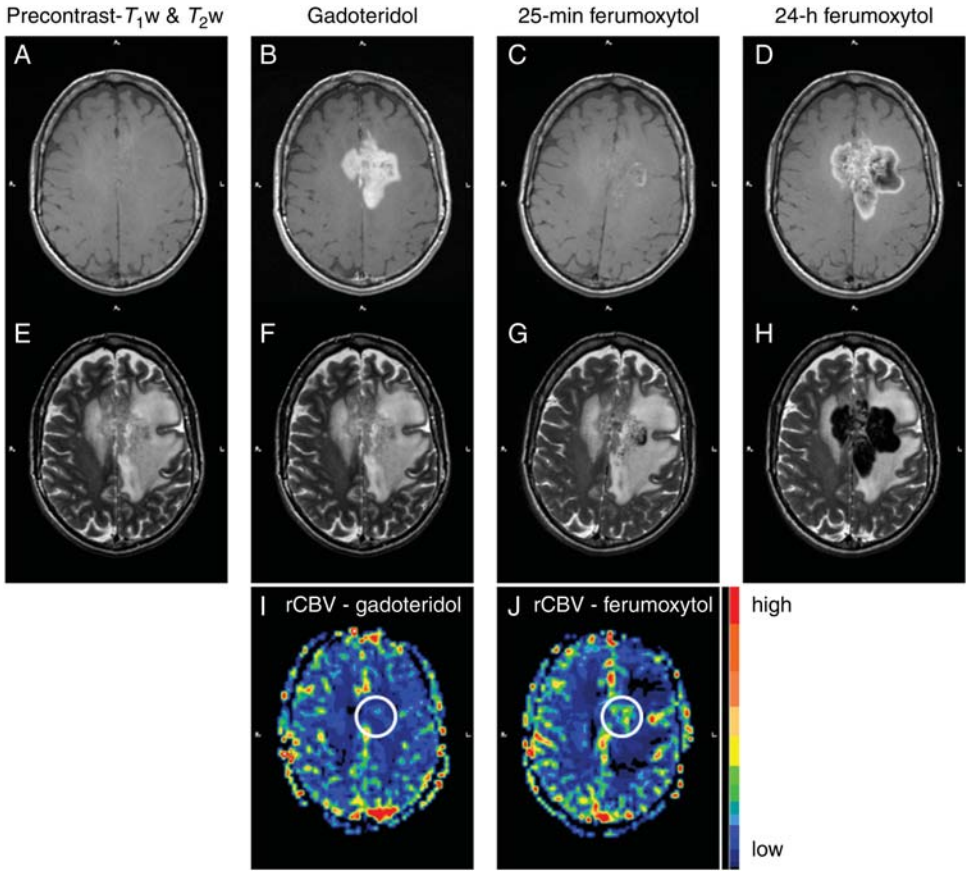

Fig. 1. Patient 8 with glioblastoma multiforme. (A and B) Nonenhanced (A) and gadoteridol-enhanced (B) T_1-weighted images of a left frontoparietal mass, which crosses the midline. The gadoteridol-enhanced image shows evidence of strong enhancement. (C) Twenty-five minutes after ferumoxytol administration, the T_1-weighted image demonstrates some faint, mainly punctate, enhancement within the mass. (D) Twenty-four hours after ferumoxytol injection, mixed SI changes are seen in the approximate region where gadoteridol enhancement is noted. (E–H) T_2-weighted images obtained before (E) and after gadoteridol (F), 25 minutes (G), and 24 hours after ferumoxytol injection (H). Twenty-five minutes after ferumoxytol administration, the T_2-weighted image shows some punctate and a curvilinear hypointensity within the mass. Twenty-four hours after ferumoxytol injection, strong lobulated areas of decreased signal are observed. The distribution of low SI areas is similar to that of mixed high and low SI areas on the T_1-weighted image in (D). (I and J) Color-coded rCBV parametric maps. The ferumoxytol-rCBV parametric map (J) shows high blood volume within the tumor, while the gadoteridol-rCBV parametric map (I) does not.

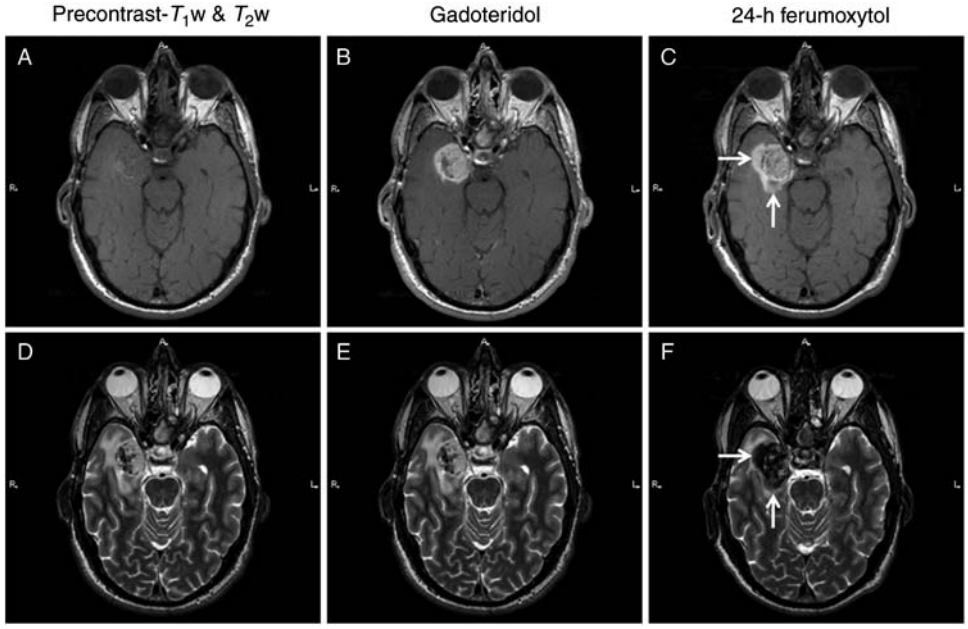

Fig. 2. Patient 6 with glioblastoma multiforme. (A–C) Nonenhanced (A), gadoteridol- (B), and ferumoxytol-enhanced (C) T_1-weighted images of a right medial temporal tumor. A linear intrinsic T_1 signal is seen in the lateral portion of the mass. The gadoteridol-enhanced image shows evidence of strong enhancement. Twenty-four hours after ferumoxytol administration, additional area of enhancement is noted around the mass (arrows), compared with the gadoteridol-enhanced images. (D–F) T_2-weighted images obtained before (D) and after gadoteridol (E) and 24 hours after ferumoxytol injection (F). Hypointense signal is demonstrated on the precontrast images in the same area where an intrinsic T_1 signal is seen. Twenty-four hours after ferumoxytol injection, strong decreased signal is observed within and around the tumor (arrows). The distribution of the low SI area is similar to that of the high SI area on the T_1-weighted image in (C).

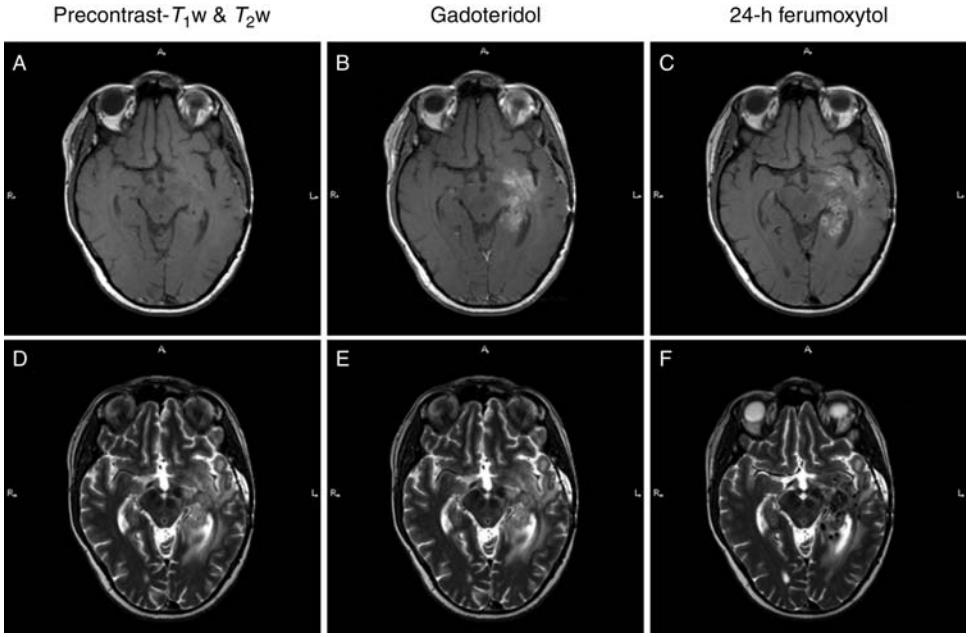

Fig. 3. Patient 3 with glioblastoma multiforme. (A–C) Nonenhanced (A), gadoteridol- (B), and ferumoxytol-enhanced (C) T_1-weighted images of a left temporal tumor. The mass is enhancing both with gadoteridol and ferumoxytol. The gadoteridol enhancement is more homogeneous compared with the punctate pattern of the 24-hour ferumoxytol enhancement. (D–F) T_2-weighted images obtained before (D) and after gadoteridol (E) and 24 hours after ferumoxytol injection (F). The ferumoxytol-enhanced image shows punctate hypointensities within the mass.

$P = .0015$; $P < .0001$, respectively) for gadoteridol compared with ferumoxytol for border delineation, visualization of internal morphology, and lesion contrast enhancement (Fig. 4).

Enhancement Volume

There was no significant difference ($P = .4471$) in enhancement volumes of the lesions [24.5 (5.0) cm^3, 22.3 (4.7) cm^3, respectively] measured on T_1-weighted gadoteridol- and 24-hour ferumoxytol-enhanced images.

CNR and SI Change

A significant difference ($P < .0001$) was demonstrated among the CNRs obtained on T_1-weighted precontrast, gadoteridol-enhanced and 24-hour ferumoxytol-enhanced images. The CNR least square means (standard errors) were 0.90 (0.04) for precontrast, 1.58 (0.04) for gadoteridol, and 1.29 (0.04) for ferumoxytol (Fig. 5A).

The mean percentages of SI changes induced by contrast agent administration on T_1-weighted images are shown in Fig. 5B. Significantly greater ($P < .0001$) SI changes were seen with gadoteridol [58.3 (5.1)%] than with ferumoxytol [28.7 (3.8)%].

Relative Cerebral Blood Volume

All 26 patients showed significant T_2^*-weighted SI decreases during each contrast agent first-pass in both lesion and normal-appearing brain tissue areas.

The ferumoxytol-rCBV values [3.73 (0.68)] were significantly higher ($P = .0016$) than the gadoteridol-rCBV values [2.52 (0.56)] (Fig. 6A).

A threshold rCBV ratio of the highest lesion blood volume to the normal-appearing contralateral white matter blood volume, measured by DSC MRI using GBCA of 1.75, has been shown to predict time to progression or survival.[10,11] Therefore, in our study, rCBV > 1.75 was considered high and rCBV < 1.75 low. The rCBV values were elevated both with ferumoxytol and gadoteridol in 14 subjects (patients 1, 2, 3, 6, 9, 11, 13, 14, 15, 16, 18, 24, 25, and 26; Table 1), although in 8 subjects the Gd-rCBV ratios were only slightly elevated compared with the 1.75 cutoff (Fig. 6B). The rCBV values were low with both contrast agents in 10 subjects (patients 5, 7, 10, 12, 17, 19, 20, 21, 22, and 23). There was a discordance between rCBV values in 2 GBM patients (subjects 4 and 8) who had elevated rCBV with ferumoxytol, but had low rCBV on the gadoteridol-rCBV parametric map (Figs 1I, J and 6B). Both participants showed worsening clinical condition and increased areas of enhancement on gadoteridol-enhanced T_1-weighted images 3 months after the study. Among those 5 patients who were treated with bevacizumab at the time of the study, 4 had low rCBV values, while 1 had elevated rCBV values with both contrast materials reflecting resistance to treatment.

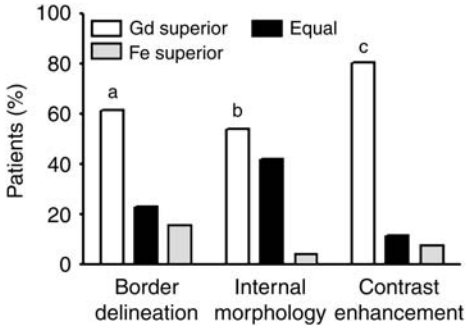

Fig. 4. Qualitative evaluation of T_1-weighted postcontrast MR images. Neuroradiologists expressed significant preferences (a, $P = .0121$; b, $P = .0015$; c, $P < .0001$, respectively) for gadoteridol compared with ferumoxytol for border delineation, internal morphology, and contrast enhancement of the lesions. The Wilcoxon signed rank test was used. Gd, gadoteridol; Fe, ferumoxytol.

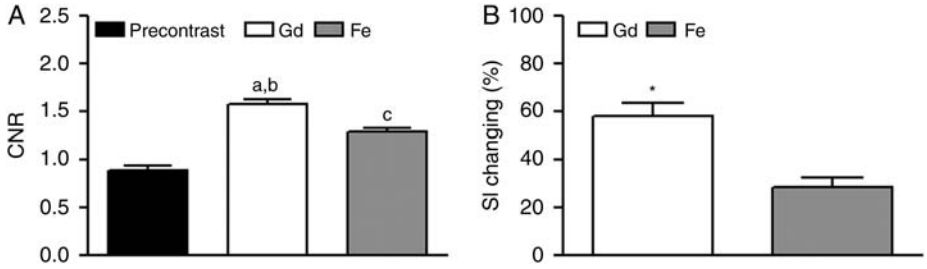

Fig. 5. Quantitation of T_1-weighted MR images. (A) A significant difference ($P < .0001$) was demonstrated among the CNRs obtained on T_1-weighted precontrast, gadoteridol-, and 24-hour ferumoxytol-enhanced images. a, $P < .0001$ for gadoteridol enhancement compared with precontrast images; b, $P < .0001$ for gadoteridol enhancement compared with ferumoxytol enhancement; c, $P < .0001$ for ferumoxytol enhancement compared with precontrast images. ANOVA and Tukey–Kramer adjustment were used. CNR, contrast-to-noise ratio; Gd, gadoteridol; Fe, ferumoxytol. (B) Significantly greater (*, $P < .0001$) SI changes were noted with gadoteridol than with ferumoxytol. The paired t-test was used. SI, signal intensity; Gd, gadoteridol; Fe, ferumoxytol.

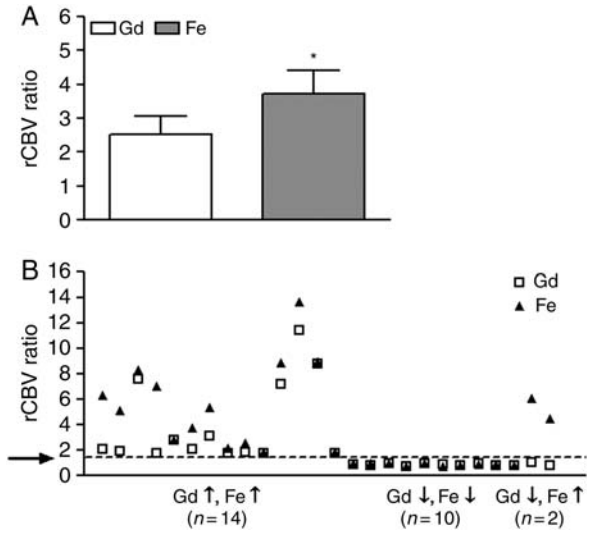

Fig. 6. Analysis of dynamic susceptibility contrast MR images. (A) The ferumoxytol-rCBV values were significantly higher (*, $P = .0016$) compared with the gadoteridol-rCBV values. The paired *t*-test was used. rCBV, relative cerebral blood volume; Gd, gadoteridol; Fe, ferumoxytol. (B) The rCBV values were elevated both with ferumoxytol and with gadoteridol in 14 patients, they were low with both contrast agents in 10, and there was a discordance between them in 2 participants. The arrow indicates a threshold rCBV ratio of 1.75. rCBV, relative cerebral blood volume; Gd, gadoteridol; Fe, ferumoxytol.

Discussion

Cerebral neoplasms are characterized by the leakiness of aberrant blood vessels and macrophage infiltration within and around the lesions, in addition to the presence of neoplastic cells. In this study, gadoteridol was used to detect vascular leakage and ferumoxytol to provide a more accurate measurement of rCBV and as a molecular agent to determine intracellular uptake within inflammatory cells in patients with intracranial tumors. These data provide insights into tumor biology and treatment effects. Elevated rCBV and minimal intracellular uptake suggest a predominance of residual or recurrent tumor, while low rCBV and increased intracellular accumulation of USPIOs would be expected within areas of suspected treatment effects.

Ferumoxytol was injected in the amount of 510 mg for all patients regardless of body weight. The intent of using a standard maximal administration was to achieve the highest possible plasma levels of ferumoxytol and thereby maximize its tissue uptake. We did not investigate the effect of ferumoxytol dose in this study. Three fundamentally different MRI sequences were used to compare gadoteridol with ferumoxytol: (1) T_1-weighted anatomical MRI, (2) T_2-weighted anatomical MRI, and (3) T_2^*-weighted DSC MRI scan. We emphasize that T_2^*-weighted SI decreases always were observed during gadoteridol and ferumoxytol first-pass DSC measurements.

USPIOs produce a hypointense signal on T_2- or T_2^*-weighted MR images in addition to T_1 enhancement.[12,13] In our study all lesions had gadoteridol and 24-hour ferumoxytol enhancement on T_1-weighted SE images. T_2 shortening consistent with iron accumulation was detected in 16 patients 24 hours after ferumoxytol administration; among them 4 showed 25-minute T_2 SI change. The USPIO-induced SI changes are known to be dose dependent. Whereas iron uptake results in T_2 shortening at higher concentrations, T_1 shortening effect peaks at lower concentrations.[12,13] Thus, at doses applied in this study, the iron accumulation was not concentrated enough to cause a decreased signal on T_2-weighted TSE images in all lesions. It is unknown whether this means that there was ferumoxytol uptake in phagocytic cells but at low concentrations or that there were not very many macrophages to endocytose USPIOs, because no histopathological analyses were performed in this study.

The exact route of USPIO entry into the CNS is not fully established. Both passive leakage of iron oxides over an impaired blood-brain barrier (BBB) and their active transcytosis through the CNS capillary membranes have been suggested to contribute to USPIO enhancement in the brain.[14,15] Although most of the nanoparticles are concentrated intracellularly according to immunohistochemical results of biopsy specimens, a small amount can also be present in the extracellular space.[7,16] This observation might explain why in 4 cases SI changes were detected as early as 25 minutes, because it is unlikely that phagocytic cells can incorporate iron nanoparticles within such a short time frame.

The 24-hour ferumoxytol enhancement covered a larger area compared with the 25-minute studies and in 6 patients extended beyond the border of the lesions delineated by gadoteridol on T_1-weighted SE images. The mechanism for this additional MRI signal change of USPIOs is most likely to be the result of intracellular trapping of iron oxides by microglia and macrophages. It should be noted that accurate brain tumor delineation is a challenging task, especially in patients with highly infiltrative tumor. Posttreatment changes may further complicate the interpretation of MR images; therefore, the true boundary of any tumor is possibly not specified by either contrast agent.

Some histopathological studies have suggested a direct association between tumor grade and number as well as location of iron-loaded microglia.[7,17] Parallel with these observations, the intensity and morphology of USPIO enhancement on MR images were found to be correlated to tumor malignancy: malignant lesions, such as high-grade gliomas, showed prominent enhancement both within and around the tumor, and particularly prominently around the necrotic areas, whereas low-grade gliomas and benign lesions, like pituitary adenomas and meningiomas, demonstrated minimal SI changes mainly at the tumor margin or showed no enhancement.[7,18] Although we noted similar tendencies in benign intracranial lesions, in patients with malignant brain tumors the morphology and intensity of ferumoxytol enhancement varied widely, presumably because of treatment-related effects.

Conventional MRI has limited ability to detect therapy-associated changes in tumor viability. Surgery

and radiochemotherapy are known to cause increased contrast enhancement due to the alteration of vascular permeability and activation of microglial cells.[19–21] On the other hand, the human antivascular endothelial growth factor monoclonal antibody bevacizumab has been shown to prune abnormal vessels and normalize existing vasculature, thus decreasing GBCA enhancement.[22] Besides its added value as a corroborative approach for achieving a diagnosis and guiding biopsies, PW MRI has also proven to be beneficial for mapping response to treatment with antiangiogenic agents.[23] Moreover, it has an essential role in differentiating tumor progression from radiochemotherapy-induced pseudoprogression as radiation necrosis typically reveals decreased rCBV within the area of abnormal enhancement, whereas high-grade tumor recurrence results in increased rCBV values.[6,24,25] Relative quantification of CBV has been found to correlate with both conventional angiographic assessments of tumor vascular density and histologic evaluation of tumor neoangiogenesis.[26,27] Despite a positive association existing between the degree of vascularity and tumor aggressiveness, some of the benign lesions (e.g. meningioma) also can be highly vascular.

The application of USPIOs may be most useful for studying tumor microvasculature. We have previously reported that rCBV estimation using ferumoxytol is reliable and does not require leakage correction.[5,8] The observed lower gadoteridol rCBV values in comparison with the ferumoxytol results in the present study are not surprising. In the case of disrupted BBB, the rapid extravasation of GBCAs from capillaries to the interstitial space leads to inaccurate CBV estimation using modeling approaches that assume contrast agents are localized only within the vascular compartment. In contrast to gadoteridol, USPIOs have a low leakage rate due to their large particle size, which makes them suitable for first-pass as well as steady-state measurements and allows precise quantification of perfusion images.

Conclusions

We have shown here that the 24-hour ferumoxytol enhancement differed from the gadoteridol enhancement in morphology and intensity. Ferumoxytol has 2 important uses that can provide additional information for brain tumor assessment either alone or in conjunction with GBCA. First, conventional MRI with ferumoxytol can detect an inflammatory component, because these nanoparticles are taken up by phagocytic cells. Second, as ferumoxytol is a blood pool agent at early time points, rCBV measurement with USPIO provides a better indicator of tumor progression than with typical GBCA, which is essential for diagnostic purposes and assessment of treatment efficacy. Beyond that, ferumoxytol has a good biocompatibility profile and has no known long-term toxicity, which makes it an attractive contrast agent for MR imaging, especially in patients with decreased renal function.

Acknowledgments

This work was supported by National Institutes of Health grants CA137488, NS53468, and ARRA CA137488-15S1, and an NCI-Fredrick Cancer Research and Development Center Contract to EAN. NIHRO1 EB007258 and NSO4801 to WDR.

Conflict of interest statement. None declared.

Funding

OHSU has received a sponsored research agreement from AMAG Pharmaceuticals to conduct clinical trials of MRI with ferumoxytol. None of the authors has financial interest in this agent or in its developer AMAG Pharmaceuticals.

References

1. Weinreb JC, Kuo PH. Nephrogenic systemic fibrosis. *Magn Reson Imaging Clin N Am.* 2009;17(1):159–167.
2. Neuwelt EA, Hamilton BE, Varallyay CG, et al. Ultrasmall superparamagnetic iron oxides (USPIOs): a future alternative magnetic resonance (MR) contrast agent for patients at risk for nephrogenic systemic fibrosis (NSF)? *Kidney Int.* 2009;75(5):465–474.
3. Weinstein JS, Varallyay CG, Dosa E, et al. Superparamagnetic iron oxide nanoparticles: diagnostic magnetic resonance imaging and potential therapeutic applications in neurooncology and central nervous system inflammatory pathologies, a review. *J Cereb Blood Flow Metab.* 2010;30(1):15–35.
4. Wu YJ, Muldoon LL, Varallyay C, et al. In vivo leukocyte labeling with intravenous ferumoxides/protamine sulfate complex and in vitro characterization for cellular magnetic resonance imaging. *Am J Physiol Cell Physiol.* 2007;293(5):C1698–1708.
5. Varallyay CG, Muldoon LL, Gahramanov S, et al. Dynamic MRI using iron oxide nanoparticles to assess early vascular effects of antiangiogenic versus corticosteroid treatment in a glioma model. *J Cereb Blood Flow Metab.* 2009;29(4):853–860.
6. Gahramanov S, Raslan AM, Muldoon LL, et al. Potential for differentiation of pseudoprogression from true tumor progression with dynamic susceptibility-weighted contrast-enhanced magnetic resonance imaging using ferumoxytol vs. gadoteridol: a pilot study. *Int J Radiat Oncol Biol Phys.* 2010.
7. Muldoon LL, Sandor M, Pinkston KE, et al. Imaging, distribution, and toxicity of superparamagnetic iron oxide magnetic resonance nanoparticles in the rat brain and intracerebral tumor. *Neurosurgery.* 2005;57(4):785–796; discussion 785–796.
8. Neuwelt EA, Varallyay CG, Manninger S, et al. The potential of ferumoxytol nanoparticle magnetic resonance imaging, perfusion, and angiography in central nervous system malignancy: a pilot study. *Neurosurgery.* 2007;60(4):601–611; discussion 611–602.
9. Spinowitz BS, Kausz AT, Baptista J, et al. Ferumoxytol for treating iron deficiency anemia in CKD. *J Am Soc Nephrol.* 2008;19(8):1599–1605.
10. Cao Y, Tsien CI, Nagesh V, et al. Survival prediction in high-grade gliomas by MRI perfusion before and during early stage of RT [corrected]. *Int J Radiat Oncol Biol Phys.* 2006;64(3):876–885.

11. Law M, Young RJ, Babb JS, et al. Gliomas: predicting time to progression or survival with cerebral blood volume measurements at dynamic susceptibility-weighted contrast-enhanced perfusion MR imaging. *Radiology*. 2008;247(2):490–498.
12. Chambon C, Clement O, Le Blanche A, et al. Superparamagnetic iron oxides as positive MR contrast agents: in vitro and in vivo evidence. *Magn Reson Imaging*. 1993;11(4):509–519.
13. Muller RN, Gillis P, Moiny F, et al. Transverse relaxivity of particulate MRI contrast media: from theories to experiments. *Magn Reson Med*. 1991;22(2):178–182; discussion 195–176.
14. Dousset V, Delalande C, Ballarino L, et al. In vivo macrophage activity imaging in the central nervous system detected by magnetic resonance. *Magn Reson Med*. 1999;41(2):329–333.
15. Rausch M, Hiestand P, Baumann D, et al. MRI-based monitoring of inflammation and tissue damage in acute and chronic relapsing EAE. *Magn Reson Med*. 2003;50(2):309–314.
16. Neuwelt EA, Varallyay P, Bago AG, et al. Imaging of iron oxide nanoparticles by MR and light microscopy in patients with malignant brain tumours. *Neuropathol Appl Neurobiol*. 2004;30(5):456–471.
17. Roggendorf W, Strupp S, Paulus W. Distribution and characterization of microglia/macrophages in human brain tumors. *Acta Neuropathol*. 1996;92(3):288–293.
18. Varallyay P, Nesbit G, Muldoon LL, et al. Comparison of two superparamagnetic viral-sized iron oxide particles ferumoxides and ferumoxtran-10 with a gadolinium chelate in imaging intracranial tumors. *AJNR Am J Neuroradiol*. 2002;23(4):510–519.
19. de Wit MC, de Bruin HG, Eijkenboom W, et al. Immediate post-radiotherapy changes in malignant glioma can mimic tumor progression. *Neurology*. 2004;63(3):535–537.
20. Kumar AJ, Leeds NE, Fuller GN, et al. Malignant gliomas: MR imaging spectrum of radiation therapy- and chemotherapy-induced necrosis of the brain after treatment. *Radiology*. 2000;217(2):377–384.
21. Vos MJ, Uitdehaag BM, Barkhof F, et al. Interobserver variability in the radiological assessment of response to chemotherapy in glioma. *Neurology*. 2003;60(5):826–830.
22. Jain RK. Normalizing tumor vasculature with anti-angiogenic therapy: a new paradigm for combination therapy. *Nat Med*. 2001;7(9):987–989.
23. Cha S, Knopp EA, Johnson G, et al. Dynamic contrast-enhanced T2-weighted MR imaging of recurrent malignant gliomas treated with thalidomide and carboplatin. *AJNR Am J Neuroradiol*. 2000;21(5):881–890.
24. Covarrubias DJ, Rosen BR, Lev MH. Dynamic magnetic resonance perfusion imaging of brain tumors. *Oncologist*. 2004;9(5):528–537.
25. Sugahara T, Korogi Y, Tomiguchi S, et al. Posttherapeutic intraaxial brain tumor: the value of perfusion-sensitive contrast-enhanced MR imaging for differentiating tumor recurrence from nonneoplastic contrast-enhancing tissue. *AJNR Am J Neuroradiol*. 2000;21(5):901–909.
26. Aronen HJ, Gazit IE, Louis DN, et al. Cerebral blood volume maps of gliomas: comparison with tumor grade and histologic findings. *Radiology*. 1994;191(1):41–51.
27. Sugahara T, Korogi Y, Kochi M, et al. Correlation of MR imaging-determined cerebral blood volume maps with histologic and angiographic determination of vascularity of gliomas. *AJR Am J Roentgenol*. 1998;171(6):1479–1486.